scientific reports

Check for updates

OPEN

Enzyme-based sensor for the real-time detection of atrazine: Evidence from electrochemical and docking studies

Simranjeet Singh[1], Pavithra N.[1], Harry Kaur[2], Radhika Varshney[1], Nadeem A. Khan[3], Rakesh Kumar[4], Ashwani Kumar Sharma[2], Joginder Singh[5] & Praveen C. Ramamurthy[1]✉

This study focused on strategically employing the carboxylesterase enzyme Ha006a, derived from the pesticide-resistant microorganism *Helicoverpa armigera*, to detect atrazine. A comprehensive analysis through biochemical, biophysical and bioinformatics approaches was conducted to determine the interaction between the Ha006a protein and the herbicide atrazine. These experimental findings elucidated the potential of leveraging the inherent pesticide sequestration mechanism of the Ha006a enzyme for sensor fabrication. Numerous optimizations were undertaken to ensure the precision, reproducibility and convenient storage of the resulting electrochemical sensor, Ha006a/MCPE. This biosensor exhibited exceptional performance in detecting atrazine, demonstrating outstanding selectivity with a lower limit of detection of 5.4 µM. The developed biosensor has emerged as a reliable and cost-effective green tool for the detection of atrazine from diverse environmental samples. The Ha006a-based biosensor fabrication has expanded the possibilities for the efficient integration of insect enzymes as analytical tools, paving the way for the design of cost-effective biosensors capable of detecting and quantifying pesticides.

Keywords Enzyme, *Helicoverpa armigera*, Atrazine, Pesticide, Biosensor

Herbicides are combinations of organic substances to prevent, eradicate or repel pests. They are used to safeguard crops and seeds in the agricultural sector and exhibit cytotoxic and carcinogenic properties, leading to respiratory ailments, neurological diseases, and human infertility[1]. The application of pesticides in relatively small regions might impact more expansive areas through their dispersion via air, water, or infiltration into the soil[2]. The chloro-triazine class of pesticides is the most widely utilized type of pesticide. Atrazine (ATZ) is the predominant insecticide in the triazine family and is used extensively in crops because of its exceptional effectiveness[3]. The half-life of ATZ in soil is 261 days, as it undergoes biodegradation by bacteria. In water, decomposition is slower due to its low solubility[4,5]. Exposure to water containing elevated levels of ATZ can result in various health issues, such as disruption of the endocrine system and hormonal balance. This raises the risk of developing breast and prostate cancer, with children being particularly vulnerable to these adverse effects[6].

Additionally, when pregnant individuals are exposed to ATZ, fetal weight decreases, and abnormalities in the urinary system, limbs, and heart develop. Prolonged exposure to high concentrations of ATZ further increases the risk of decreased survival. As per the US Environmental Protection Agency, the permissible limit for ATZ concentration in drinking water is 3 ppb[7]. However, even prolonged exposure to such low quantities significantly impacts the human endocrine system. Due to the detrimental impact of ATZ on the ecosystem, it is advantageous to develop or fabricate biosensor platforms capable of qualitatively and quantitatively detecting ATZ in water.

[1]Interdisciplinary Centre for Water Research (ICWaR), Indian Institute of Science, Bengaluru, Karnataka, India. [2]Department of Biosciences and Bioengineering, Indian Institute of Technology Roorkee, Roorkee 247667, India. [3]Interdisciplinary Research Center for Membranes and Water Security (IRC-MWS), King Fahd University of Petroleum and Minerals, Dhahran 31261, Saudi Arabia. [4]Division of Crop Improvement, ICAR-Central Institute for Cotton Research (ICAR-CICR), Nagpur, Maharashtra, India. [5]Department of Botany, Nagaland University, Hqrs. Lumami, Nagaland, India. ✉email: onegroupb203@gmail.com

Due to the ecotoxicological implications of ATZ's presence in environmental and food matrices, an increasing number of approaches have been employed, including gas chromatography (GC), high-performance liquid chromatography, GC equipped with MS, and capillary zone electrophoresis to monitor the traces of ATZ[8–10]. These approaches are costly, labour-intensive, occasionally necessitate pre-concentration or extraction procedures and are unsuitable for in situ monitoring applications. The research has mainly focused on developing portable, highly responsive, cost-effective sensors.

The primary method for detecting pesticides in an electrochemical biosensing system relies on directly identifying electroactive pesticides or utilizing enzymes, bacterial species and antibodies as receptors for biodetection[11]. Electrochemical biosensors have garnered significant interest because of their exceptional specificity and sensitivity[12]. The critical component of these sensors is the receptor, which refers to the biological molecular recognition element capable of selectively binding to the analyte. The receptor is directly near a transducer, typically amperometry or potentiometric, which can transform the bio-recognition event into a measurable signal[13]. Few studies have documented the use of biological molecules for the detection of atrazine[14–18].

Presently, there is a research gap pertaining to the utilization of enzymes in sensors dedicated to the analysis of organochlorines. Thus, it becomes imperative to delve into and advance the exploration of green sensors tailored explicitly for the detection of triazine pesticides. To overcome this, we have isolated the carboxylesterase enzyme (Ha006a) from an agricultural pest, *Helicoverpa armigera* and strategically utilized it to synthesize a green enzyme-based sensor that exhibited elevated sensitivity and selectivity in detecting ATZ. This study highlights the efficacy of incorporating green materials in the realm of electrochemical ATZ detection. This study encapsulates the conceptualization, fabrication and evaluation of an enzyme-based biosensor designed to precisely detect and quantify atrazine levels. A comparative analysis has been systematically undertaken to scrutinize the biosensor's response. Additionally, the stability of the biosensor has been meticulously assessed to ascertain its robustness under varying storage conditions.

Methodology

Materials

All the chemicals were procured from HiMedia. The chromatography columns were purchased from GE Healthcare. Atrazine was procured from Sigma Aldrich Bengaluru (KA). The protein ladder used in this study was acquired from Thermo Scientific, USA.

Purification and expression of Ha006a protein

The plasmid construct of pET32a::Ha006a in the *E. coli* Rosetta (DE3) host was sourced from IIT Roorkee. Expression and purification of the recombinant Ha006a enzyme followed a previously established protocol[19]. Briefly, a single colony of Rosetta (DE3)-pET32a::Ha006a was cultured in 10 mL of Luria–Bertani (LB) broth and incubated overnight at 37 °C at 200 rpm. Subsequently, a 1-L LB secondary culture supplemented with appropriate antibiotics was inoculated, and growth was monitored until it reached an OD_{600} of 0.6–0.8. Induction of Ha006a overexpression was achieved by incorporating IPTG and incubating for 18 h at 16 °C with shaking (200 rpm).

Chromatography techniques such as Ni-NTA affinity and anion exchange chromatography were employed to obtain the target protein in soluble fractions. The Ha006a protein was purified using HIS-Select HF Ni-NTA affinity chromatography followed by anion exchange chromatography, following protocol[19]. Briefly, after centrifugation, cells were collected and vortexed thoroughly in purification buffer (50 mM Tris–HCl, 300 mM NaCl, and 5% (v/v) glycerol) and subjected to a single pass through a French press (Constant Systems Ltd., England) at 21 psi for 60 s, and centrifuged to obtain debris free supernatant. The clarified lysate was then applied to pre-equilibrated Ni-NTA resin, and bound Ha006a was purified following a stepwise gradient of imidazole (5–250 mM). The eluted fractions were loaded on 12% SDS-PAGE to visualise the eluted content. The purified Ha006a protein was then dialyzed against purification buffer but with a lower concentration of NaCl (150 mM) to remove N-terminal ThioredoxinA (Trx) solubility and 6x-His tags via Tobacco Etch Virus (TEV) protease digestion. The tag-cleaved Ha006a fraction was purified by anion exchange chromatography using 50 mM Tris–HCl buffer and 10% (v/v) glycerol. The pI of Ha006a protein is 4.56, so the buffer composition was maintained at pH 7.5 to ensure the negatively charged protein binds efficiently to the DEAE-Sephadex electrostatically. The eluted protein fraction was concentrated to approximately 2.5 mL using a 10 kDa concentrator (Millipore, USA) and quantified by UV spectrophotometry at 280 nm.

Molecular docking and dynamic simulation

The open reading frame of Ha006a (GenBank® accession number PP204289.1) was retrieved from NCBI, and a high-quality 3D protein model was generated using AlphaFold v2.1.1[20]. The parameters considered for selecting the best model were the Ramachandran plot and the angles. The other factors that were considered in the quality assessment were the MolProbity score and the Clash score. The stereochemical stability of the generated model was further analyzed with the aid of the SAVES server.

The active site residues of Ha006a were identified using the conserved domain search tool in the NCBI database[21]. The ligand structure, ATZ, was procured from PubChem[22]. The energy of ATZ was minimized with the Universal force field (uff) in the Open Babel software[23]. The 100 ns simulated AlphaFold model of Ha006a was subjected to a docking process. The Ha006a was prepared for the in-silico study by adding polar hydrogen and Kollman charges, and the pdb file was converted to PDBQT in AutoDock module[24]. Molecular docking serves as a pivotal tool within the realm of computational chemistry, facilitating an in-depth exploration of the intricate geometrical and conformational aspects inherent to protein–ligand interactions. This methodological

approach enables a comprehensive investigation to get insights into the binding energy and flexibility of the interacting molecules[25].

Docking was conducted using AutoDock vina, and the binding affinity (kcal/mol) was computed. The characteristics of substrate binding pocket and the catalytic triad residues consisting of Gly106, Gly107, Gly108, Glu186, Ser187, Ala188, Ala191, Glu309, Phe331, Tyr335, Phe336, His372, His423, Ala424, and Leu427 were selected to create the docking receptor grid. Docked structures were thoroughly analyzed in PyMOL[26], and interactions were monitored to determine the most favourable conformation adjusting in the active site.

The CHARMM36 forcefield was used to generate the topology files, and Ha006a was further solvated using TIP3P option[27]. In the Avogadro v1.2.0 software, the hydrogen atoms were added to the atrazine structure[28]. The ligand parameter and topology files were prepared using the CHARMM General Force Field (CGenFF) server[29]. The Ha006a and its ligand, ATZ, were centred within a cubic box with padding of 1.5 nm and solvated by the SPC water module. Neutralization was performed using Na^+/Cl^- ions and further subjected to energy minimization employing the steepest descent approach for 100 ps with 50,000 nsteps. The system was equilibrated at temperature and pressure of 300 K and 1 bar, respectively, for 100 ps. The protein–ligand complex was ultimately introduced to a molecular dynamic simulation run of 100 ns[30].

Inhibition assay

The inhibitory impact of ATZ on the Ha006a enzyme was assessed in vitro, as outlined in a recent study[19]. The pure Ha006a enzyme (0.2 nM) was mixed with different quantities of ATZ (10 µM–10^3 µM) in a 1 µL solution and incubated for ten minutes at 35 °C. Blanks were made without the addition of Ha006a enzyme and reaction controls were maintained by substituting 1 µL of the solvent for ATZ. The inhibition experiment was stopped by introducing 10 µM substrate, α-naphthyl acetate (α-NA) and then the measurements were examined at 450 nm. The IC_{50}, representing half inhibitory concentrations, was calculated by employing this equation[19]:

$$\%\ Inhibition\ of\ enzyme\ activity = \frac{Absorbance\ without\ I - Absorbance\ with\ I}{Absorbance\ without\ I} \times 100$$

The 'absorbance without I' indicates the absorbance of the reaction devoid of the inhibitor, ATZ, while keeping all other parameters constant compared to the reaction mixture with the inhibitor. Enzyme inhibition percentage was then determined using linear regression fitting, and the equation $Y = mX + c$, was used to compute the X variable. Triplicates were maintained for each concentration, and a linear regression graph was generated using Origin 7.0 software.

Biophysical characterization

The label-free gold standard technique, ITC, is widely employed to determine the protein–ligand interaction profile[31]. This technique effectively monitors the thermodynamic parameters of the interaction on gradual titration. To investigate the interaction between the Ha006a protein and ATZ, Isothermal Titration Calorimetry (ITC) experiment was conducted at 25 °C jacket temperature. The protein (30 µM) was filtered, degassed, and introduced into the sample cell of the MicroCal iTC-200 instrument (GE Healthcare). Simultaneously, the titrant, ATZ (60 µM), was prepared in the same buffer, processed similarly, and loaded into the syringe. The buffer maintained for this experiment consisted of 10 mM sodium phosphate and 100 mM NaCl, having a pH of 7.5. A series of 20 injections were administered, with an initial ligand volume of 0.4 µL with a duration set as 1 s and subsequent injections of 2 µL volume with a duration of 4 s. A 60-s initial delay was applied and the syringe stirring speed was maintained at 750 rpm. A spacing of 200 s and a filter period of 5 s was maintained throughout the titration experiment. Heat change was calculated with the reference compartment maintained at 8.0 µW and data interpretation was done in the Origin 7.0 platform. The ITC data was analyzed employing a one-site binding model, yielding the thermodynamic profile on interaction. The ITC experiment aimed to ascertain the presence of interaction and further utilize it in biosensor development; thus, a consistent molar ratio of 1:2 (protein to titrant) was maintained in this experiment. ITC isothermogram revealed two graphs: one graph showcasing the raw data of differential power v/s time, while another panel depicting the processed data revealing the plot of heat v/s molar ratio inside the compartment. The thermodynamic profile, namely, change in enthalpy, entropy and binding free energy, equilibrium dissociation constant (Kd), and the stoichiometry (n) during the interaction, was determined by this experiment.

Electrochemical instrumentation and fabrication of electrodes

The CHI660D electrochemical system (CH Instruments Inc., Austin) was used to perform cyclic voltammetry (CV) and differential pulse voltammetry (DPV) analysis. The experiment utilized a three-electrode setup design with a carbon paste electrode (CPE) as the working electrode. The potential and current monitoring of all samples were performed in comparison to a saturated calomel electrode (SCE) and platinum wire, which functioned as the reference and counter electrodes, respectively. A bare carbon paste electrode (BCPE) was created by mixing 0.24 g of graphite fine powder with 0.04 mL of silicone oil until a homogenous paste was achieved. The paste was loaded on the loop of the CPE electrode and settled to create a polished look on the electrode.

Furthermore, it was brought in contact with the CHI apparatus via a copper cable. A modified carbon paste electrode (MCPE) was generated by combining 10 µM of Ha006a protein, 0.24 g of powdered graphite, and 0.04 mL of silicone oil to make a homogenous paste. The MCPE was prepared similarly to BCPE but with an enzyme added to its mixture. The electrochemical tests were executed using a 1 µM HCl acid buffer solution.

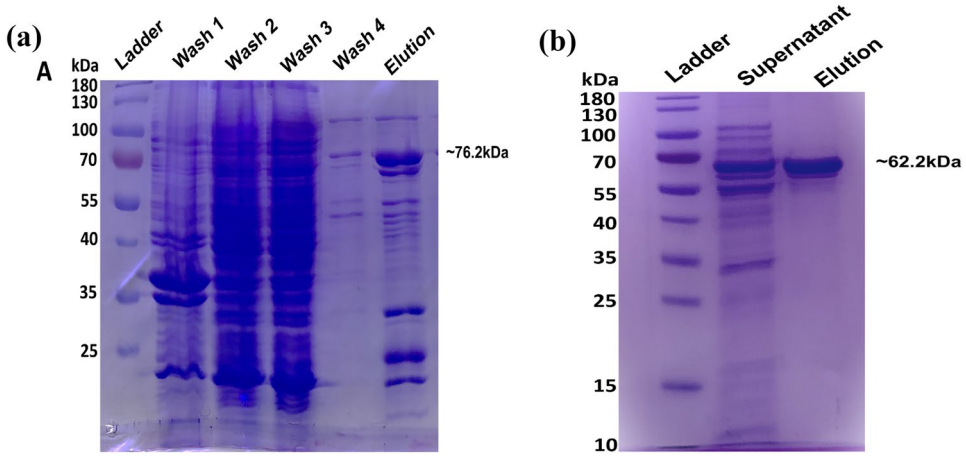

Figure 1:. 12% SDS-PAGE revealing the purification of Ha006a protein by employing chromatography techniques. In both the gels, Ladder: Protein Ladder (Thermo Scientific) was loaded. (**a**) Purification was performed using the Ni-NTA affinity chromatography technique. The gel bears witness to a gradient of imidazole, identified as follows: First wash with 5 mM imidazole, second with 10 mM, Third with 15 mM, then with 20 mM, and the elution with 250 mM imidazole. (**b**) Purification was performed by anion exchange chromatography. In the gel, supernatant signifies the flow-through obtained as the initial passage through the column and the elution reveals the purified Ha006a protein, achieved with a buffer containing 300 mM NaCl. The original gel images are available in the supplementary file (Fig. S1 and S2).

Results and discussion

Purification and optimization of Haoo6a protein

The Ni-NTA affinity chromatography technique was adopted to obtain elution of the Ha006a protein along with the N-terminal Trx and 6x-His tags intact. The eluted protein of ~ 76.2 kDa was observed in the SDS-PAGE (Fig. 1a). The Ha006a protein was subjected to dialysis with TEV protease to detach the tags. Subsequently, the dialyzed protein after reverse Ni-NTA chromatography steps was purified by anion exchange chromatography. The second chromatography exhibited a distinct band ~ 62.2 kDa (Fig. 1b), indicative of the high degree of purity.

Molecular docking for Ha006a–atrazine

Molecular docking was performed to understand and obtain valuable insights into the orientation and molecular interaction of atrazine with Ha006a protein in the AutoDock tools platform of the MGL tools suite v1.5.6. The outcomes derived from the molecular docking analysis demonstrated that ATZ exhibited robust positional stability within the active site of Ha006a, primarily attributed to the establishment of significant interactions (Fig. 2a). ATZ established essential interactions with the critical active site residue, including Ser187, Ala188, Ala191 and His423 within the binding pocket. The catalytic triad residues Ser187, Glu309 and His423 formed significant interaction with ATZ; among the three, the Glu309 residue exhibited polar contact with the ligand. The other interacting residues within the vicinity of 4 Å were Phe109, Ser212, Gly213, Ala214, Ser217, Trp219, Ala220, Tyr312, Phe376, Phe377, Pro380 and Val381 (Fig. 2b). Hence, the molecular dynamics outcome elucidated the noteworthy interacting residues within the active site, thereby confirming the robustness of the interaction.

Molecular dynamic simulation of Ha006a–atrazine interaction

The protein in native form and complex with ATZ was subjected to a molecular dynamic simulation run for 100 ns. Several parameters considering the fluctuations and displacement of the protein from its initial position were investigated to monitor the structural stability of the Ha006a–ATZ complex. The outputs of atomic trajectories were analyzed to determine the conformation of the protein structure. Root Mean Square Deviation (RMSD) is a fundamental metric to analyze and evaluate the overall structural deviation in context to the Cα-backbone of the protein in silico condition. The RMSD values for apo Ha006a and the Ha006a- ATZ complex were 0.166 nm and 0.262 nm, respectively. These results indicate that ATZ preserved a stable conformation when bound to the Ha006a protein (Fig. 3a). The Root Mean Square Fluctuation (RMSF) value helps to monitor and quantify the fluctuation of Cα atom coordinates of the individual residues from the average position to accommodate the ligand throughout MD trajectory. The RMSF obtained were 0.120 nm and 0.150 nm for apo Ha006a and Ha006a–atrazine complex, respectively. The RMSF plot exhibited higher flexibility, revealing that ATZ fits nicely into the binding pocket of the protein (Fig. 3b). Solvent Accessible Surface Area (SASA) analysis plays a pivotal role in understanding the solvent accessible to the protein surface throughout the simulation run.

Owing to the conformational changes during the simulation, the surface area of protein exposed to the solvent molecules gets altered, which provides insights into the stability of the underlying interaction mechanisms. This study provided valuable information about compactness and the extent of solvent accessibility. The values of SASA measured for Ha006a and Ha006a–atrazine complex were 240.5 and 257.9 nm^2, respectively (Fig. 3c). The Ha006a–atrazine complex exhibited higher SASA value, which signified that the complex was more favourable

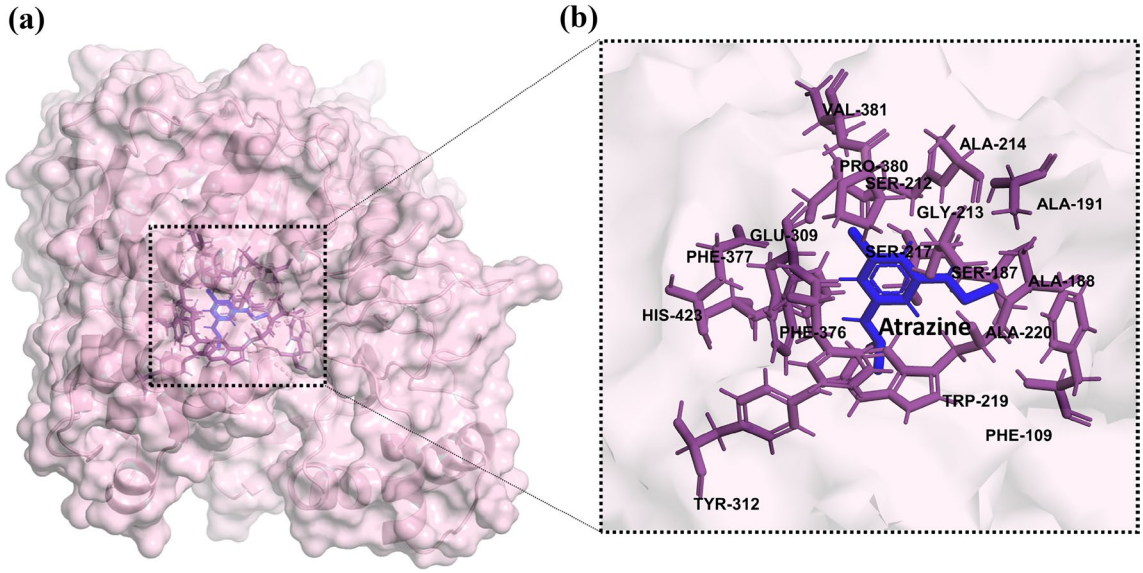

Figure 2. Interaction of atrazine with Ha006a protein. (**a**) The Ha006a protein is depicted as in surface form, and the active site residues are displayed in the stick form. Atrazine (blue) is buried in the substrate binding pocket of the protein. (**b**) The substrate binding residues are in the form of sticks (purple) and are labeled for better illustration.

as compared to the native state of the protein. The Radius of Gyration (Rg) analysis was also performed to unravel how extended or compact the protein is from its centre of mass in three-dimensional space. Rg values of Ha006a in native and complex states were 2.37 nm and 2.02 nm, respectively. The Rg plot inferred that the Ha006a–atrazine complex possesses greater compactness and hence, higher stability (Fig. 3d). Furthermore, the hydrogen bonds formed between Ha006a and ATZ throughout a run of 100 ns were evaluated and graphically illustrated. The formation of the H-bond was observed in the range of 0–4 owing to robust interaction (Fig. 3e). The hydrogen bond profiling play a critical role in overall protein folding and primarily contribute to enhancing binding affinities.

Moreover, the interaction energy between protein and ligand in the form of coulombic and Lennard–Jones (LJ) potentials was computed. LJ potential was − 37.66 kJ/mol and Coulombic interaction energy was − 320.71 kJ/mol for the Ha006a–ATZ complex. Thus, it exhibited low non-bonded interaction energy, 358.37 kJ/mol, to form a complex with Ha006a. The computational analysis, including the docking and simulation studies, confirms that ATZ binds to the substrate-binding site of Ha006a and acts as its potent inhibitor. It was observed that ATZ formed three hydrogen bonds and required low Van der Waals energy as well as higher electrostatic interaction energy for binding to Ha006a.

Moreover, ATZ exhibited polar contact with the Glu309 residue, which is one of the essential amino acids forming the catalytic triad of Ha006a. The amino group (NH_2) of ATZ revealed polar interaction with the oxygen atom of Glu309 at a distance of 1.6 Å (Fig. S3). This interaction encouraged the transfer of a partial positive charge from the amino group to the oxygen atom, creating a partial negative charge on the amino group and a partial positive charge on the oxygen atom. These charge transfers are transduced into an electrical signal leading to a detectable peak or change in signal intensity. Thus, the overall results suggest that the Ha006a–ATZ complex leads to the formation of a stable complex and, hence, competitively inhibits the enzyme by binding to its substrate binding site. The biophysical and inhibition assay further supports the bioinformatics findings and validates our report. Moreover, delving into enzyme kinetics extensively could justify the inhibition mechanism.

Enzyme activity and IC_{50} detection

To gain an understanding of the esterase activity of Ha006a, we employed alpha-naphthyl acetate (α-NA) as a natural substrate. In our previous study, Ha006a was found to have a high affinity for alpha-naphthyl acetate and reported a Km value of 10.88 ± 0.54 μM[19]. The IC_{50} value for the well-established CarE inhibitor TPP against Ha006a was documented as 428.5 ± 13.23 μM[19]. It was observed that ATZ exhibited significant inhibitory effects on Ha006a and the analysis was carried out in triplicates. The IC_{50} value was calculated as 224.66 μM ± 15.01, indicating the concentration of ATZ needed to achieve a 50% reduction in Ha006a esterase activity (Fig. 4). This investigation strongly confirms that the inhibitory potency of atrazine on Ha006a catalytic activity was higher as compared to the reported inhibitor, TPP.

Isothermal titration calorimetry (ITC)

The Ha006a–atrazine interaction study was conducted employing the ITC technique. The isotherm depicted that the Ha006a–atrazine binding was exothermic and was enthalpy-driven with a dissociation constant (Kd) of 57 μM showing ΔH and ΔS values of $-5.534E^6 \pm 4.919E^5$ cal/mol and $-1.85E^4$ cal/mol/deg respectively (Fig. 5a).

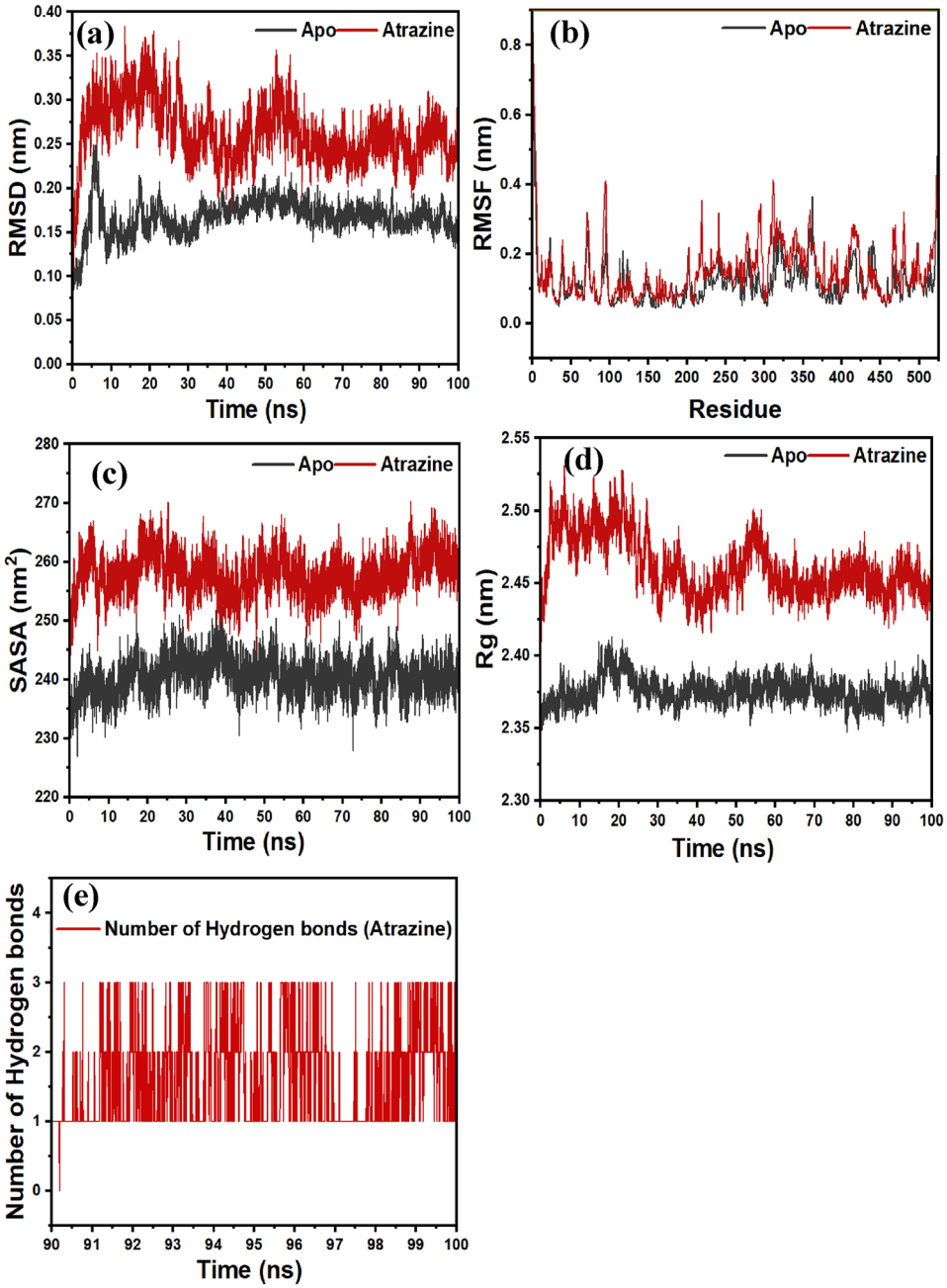

Figure 3. The analysis of the graphs after a molecular dynamic simulation run of 100 ns of the apo Ha006a and in complex with atrazine. The structural stability of the apo Ha006a and the complex is plotted in the form of (**a**) RMSD, (**b**) RMSF, (**c**) SASA, (**d**) Rg, and (**e**) Number of hydrogen bonds. The graphical representation includes the apoprotein in black and the complex in maroon.

The other thermodynamic parameters were calculated during the interaction (Fig. 5b). The entropy factor (TΔS) and the enthalpy change depicted that the interaction encompasses a combination of non-covalent interactions, thereby rendering the reaction favourable. The non-covalent interactions may be hydrogen bonds, hydrophobic interactions, or Van der Waals forces. Enthalpy change (ΔH) in the molecular interaction process typically determines the strength of non-covalent interactions[32]. The overall biomolecular interaction provides valuable insights revealing the stability, the bonds involved, and the strength between the two entities[33]. The existing research suggests that enthalpy-driven ligands confer high selectivity and possess higher binding affinities[34]. Considering these factors, the Ha006a- ATZ binding profile was observed to reveal intermolecular solid interactions, thereby depicting higher conformational flexibility and specificity.

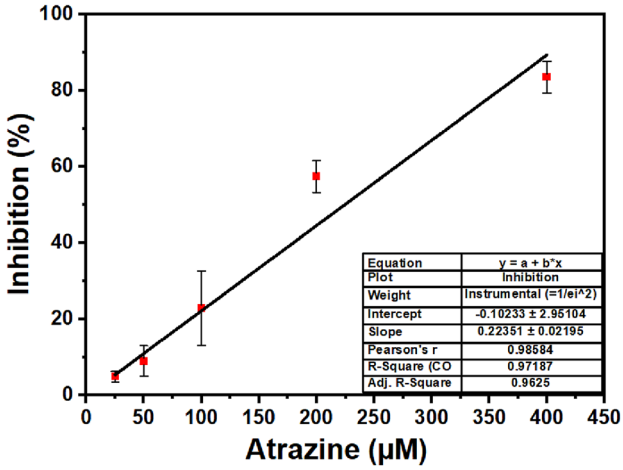

Figure 4. Inhibition assay to calculate IC_{50} value. The figure illustrates the interaction between Ha006a and atrazine, highlighting the inhibitory effect. The readings were monitored in triplicates, and the standard deviation is denoted as horizontal bars.

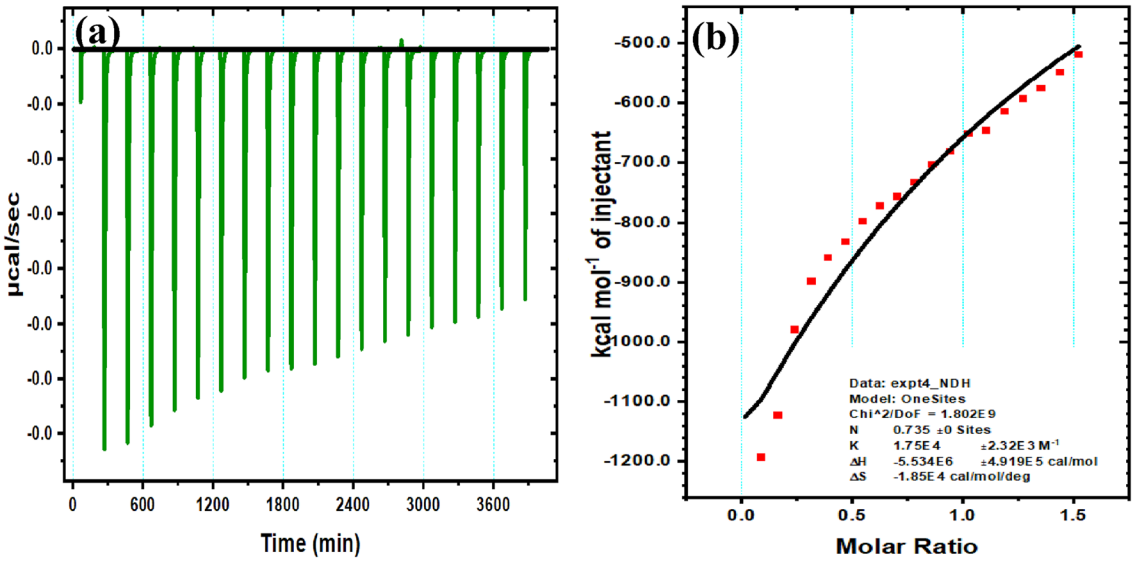

Figure 5. The isothermogram generated by ITC was utilized to analyze the binding of Ha006a with atrazine. Ha006a (30 µM) in the cell was titrated against atrazine (60 µM) with gradual injections from the syringe. (**a**) Illustrating the differential power versus time, and (**b**) graph depicts the injection heat plotted against the molar ratio in the cell.

Analytical behaviour of Ha006a modified electrode towards atrazine detection

The differential pulse voltammetry (DPV) approach was employed to electrochemically detect ATZ, utilizing 1 µM HCl solution as the electrolyte. Figure 6a illustrates the oxidation reaction of Ha006a/MCPE with atrazine. To confirm the electrochemical properties discussed earlier, the reactions of BCPE and MCPE to atrazine (50 µM) were assessed using the DPV method at a scan rate of 50 mV/s. BCPE had a peak current of around 0, whereas MCPE had a current intensity of 1 µA at a potential of 0.28 V. The results demonstrate the exceptional catalytic performance of Ha006a in relation to ATZ.

Experimental optimization

The optimum experimental parameters were set to ensure the best performance of fabricated sensors. To improve the analytical efficiency, the impact of scan rate, types of electrolytes, and the concentration of ATZ were validated by fabricating the Ha006a/MCPE.

Impact of scan rate

The scan rate of the Ha006a/MCPE electrode in response to ATZ (50 µM) was investigated using cyclic voltammetry. The scan ranged from 0.0–0.8 V, maintaining a constant atrazine concentration of 100 µM. The electrolyte

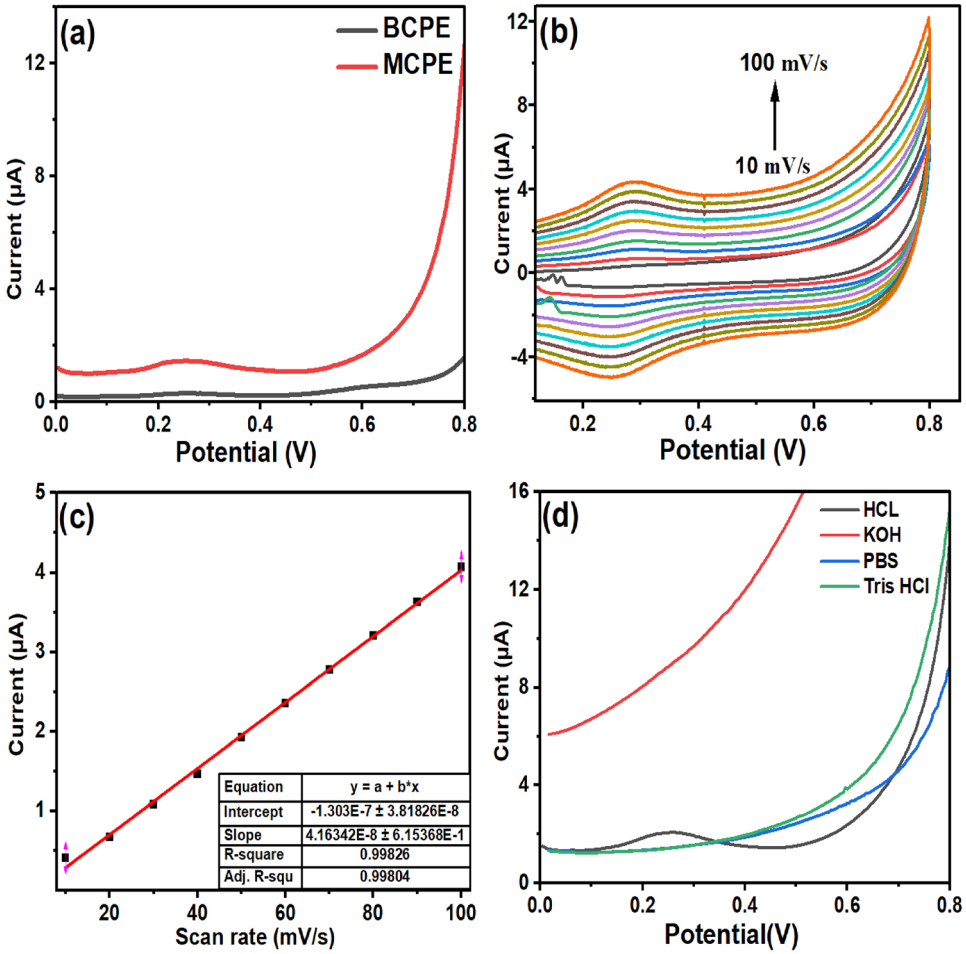

Figure 6. Graphs depicting the optimization of experimental parameters (**a**) DPV plots of the modified Ha006a/MCPE towards atrazine, (**b**) Effect of scan rate on the modified Ha006a/MCPE, (**c**) Regression plot of scan rate versus current, (**d**) Effect of buffer on the modified Ha006a/MCPE.

solution included 1 μM HCl and the scan rate in the range of 10–100 mV/S. Figure 6b demonstrates that both redox peaks exhibit an augmentation as the scan rate increases. Figure 6c displays the graph of the anodic peak current as a function of the scan rate. The graph exhibits a robust linear relationship, as indicated by the linear equation ($Ia = 4.16\ E^{-8}\ (v) - 1.36\ E^{-7}$). The correlation coefficient (R^2) was calculated to be 0.99, indicating a high degree of connection between the variables.

Impact of electrolyte

The selectivity of electrolytes in electroanalytical research is crucial for accurately determining the charge transport of electrons. Diffusion occurs due to a difference in concentration, leading to the movement of analytes from regions of high concentration to regions of low concentration. Theoretical analysis and simulations neglect the migration and convection of the analyte. The reduction of convection is achieved by avoiding stirring or vibrations, whereas the reduction of migration is achieved by employing a highly concentrated electrolyte. Hence, the electrolyte's nature in relation to the concentration of the analyte significantly increases the probability of the electrolyte migrating to the electrode surface to create equilibrium in charges, thereby regulating the electron movement process. The reaction of MCPE to atrazine at a concentration of 50 μM was investigated using four different electrolytes: 1 μM HCl, 0.1 M Tris HCl, 1 M PBS and 1 M KOH buffer. The potential range used was from 0 to 0.8 V. The results of this study are presented in Fig. 6d. The potassium hydroxide buffer exhibited a superior current compared to other buffers. However, no notable peak was detected. An evident peak was seen at a potential of 0.24 V with respect to ATZ in the HCl buffer. Consequently, HCl buffer with a concentration of 0.001 mM was used for subsequent experiments.

Impact of concentration variation

The DPV approach was employed to illustrate the impact of concentration variations at the Ha006a/MCPE. Figure 7a displays the differential pulse voltammetry (DPV) plots acquired for ATZ in the supporting electrolyte, 1 μM HCl. The peak current exhibits a direct proportionality to the rise in atrazine concentration in the range of 10–100 μM, resulting in a corresponding increase at 0.32 V. The peak current for each concentration was obtained

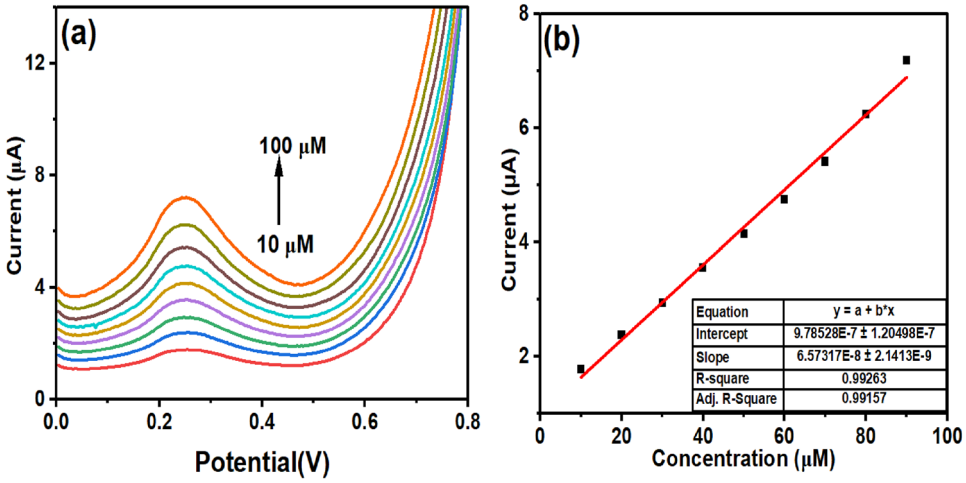

Figure 7. Differential Pulse Voltammetry (DPV) graphs to analyze the effect of atrazine concentration. (**a**) DPV plots of concentration variation on the modified Ha006a/MCPE, (**b**) regression plot concentration versus current.

by preparing fresh electrodes each time. The increasing peak current was observed with the increase in concentration of ATZ, both in the presence and absence of substrate. This implies that the inhibition type potentially demonstrated by ATZ was competitive inhibition. This proves that the electron transfer between the enzyme of the modified electrode increases the electrical conductivity even in the presence of interfering molecules. Additionally, Fig. 7b illustrates the correlation between the peak current and the concentration change using the equation ($I = 6.5\ E^{-8}$ (conc.) + $9.7\ E^{-7}$, linear), with a correlation coefficient (R^2) of 0.99. In addition, the limit of detection (LOD) was calculated using 3*SD/Slope of the obtained equation from Fig. 7b and found to be 5.4 µM.

Table 1 presents a comparison of the analytical performance of the proposed method with previously published electrochemical methods for determining ATZ. Several articles have been published that focus on finding electrode surfaces that are both ecologically acceptable and capable of reducing ATZ with good sensitivity, repeatability and cheap cost. The objective is to achieve this without increasing the production of toxic waste.

The developed sensor (Ha006a/MCPE) exhibits an exceptional limit of detection (LOD) of 5.4 µM for ATZ, significantly surpassing the 20 µM LOD of cell-free sensors[16]. Furthermore, our developed sensor demonstrates high LOD compared to biosensors employing Ana-1 cells and aptamers for ATZ detection[35,36]. Compared to other materials listed in Table 1, which predominantly consist of nanoparticles, nanofibers, or molecularly imprinted polymers (MIPs), the developed sensors offer a notably lower LOD. Further optimization of sensor characteristics and synthesis procedures will be made to increase the sensitivity towards atrazine detection. Moreover, our developed sensors exhibit high selectivity, sensitivity, and recovery rates (ranging from 95.66 to 98.66%) across various matrices, effectively detecting ATZ in different environmental contexts (Supplementary Figures).

Reproducibility, selectivity, and stability of Ha006a/MCPE towards atrazine detection

The electrode's repeatability was assessed using the Differential Pulse Voltammetry (DPV) technique, employing Hydrochloric Acid (HCl) buffer with a concentration of 1 µM. The concentration of ATZ was set at 100 µM. The

Electrode	Linear range	Limit of detection	References
SiO_2@atrazine-MIP nanoparticles	–	1.8 µM	18
GNPs	0.05 µM and 0.5 µM	0.016 µM	17
Cell-free sensor	–	20 µM	16
Ana-1 cells	10^3–5×10^4 µM	150 µM	35
Aptamer	50–10^4 µM	35 µM	36
MIP-based screen-printed potentiometric cell	0.5–50 µM	0.4 µM	13
Tyrosinase immobilization on polyvinyl alcohol with styryl-pyridinium groups	10–100 µM	1.3 µM	14
Electro-spun SnO_2 nanofiber	1^{-15} µM to 1 µM	9×10^{-16} µM	37
Molecularly imprinted conducting polymer	1 nM–100 µM	0.4 µM	38
Boron-doped diamond electrode	0.05–40 µM	0.01 µM	15
Ha006a/MCPE	10 µM–100 µM	5.4 µM	Present work

Table 1. Comparison of developed sensor platforms with previously reported literature.

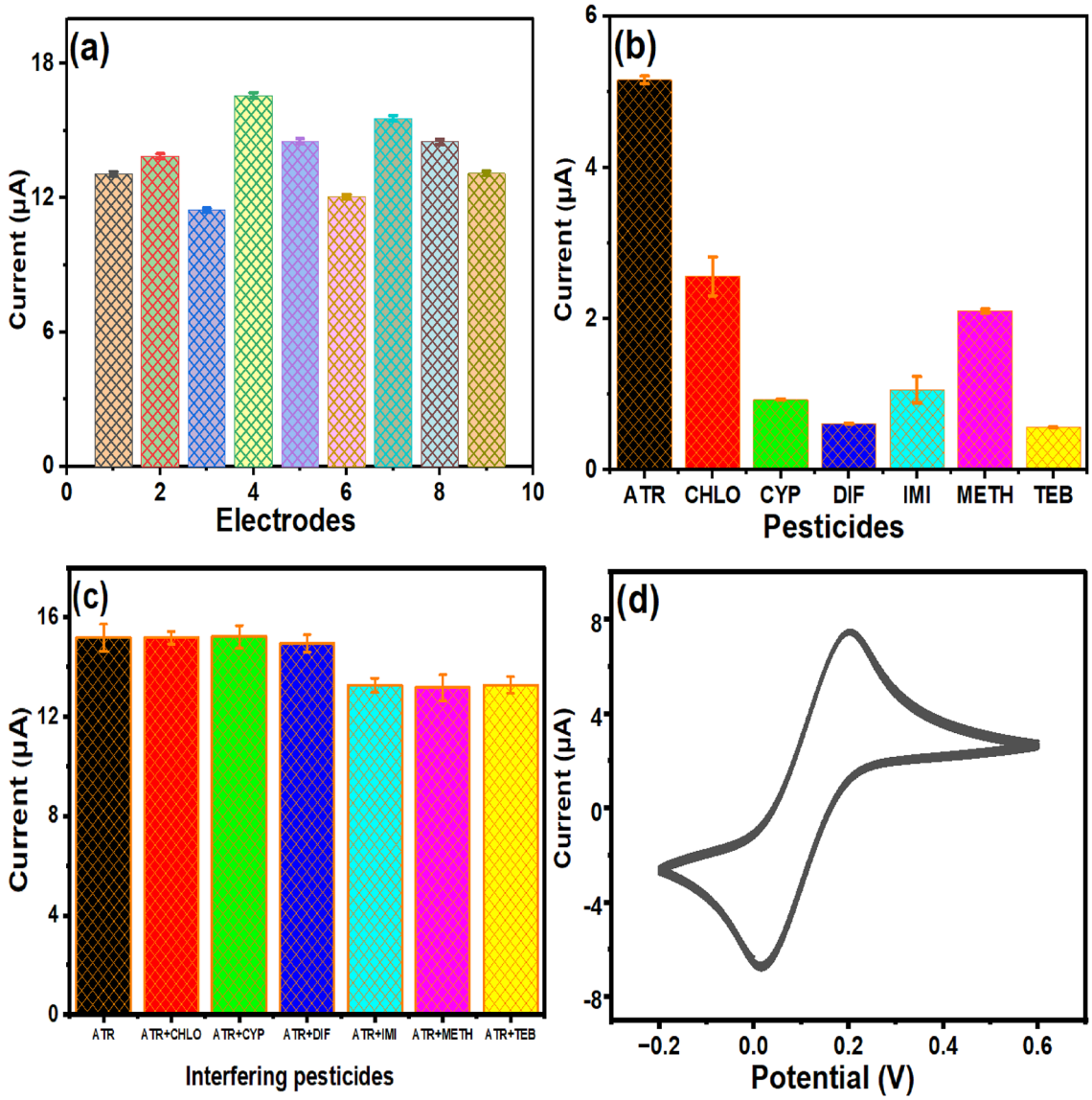

Figure 8. Plots depicting stability of Ha006a/MCPE towards atrazine detection (**a**) Repeatability of modified Ha006a/MCPE in 1 µM HCl buffer, (**b**) Selectivity of modified Ha006a/MCPE in 1 µM HCl buffer, (**c**) Effect of different interferants in 1 µM HCl buffer, (**d**) Stability of modified Ha006a/MCPE (KCl- 0.1 M).

figure labeled as Fig. 8a displays the peak current intensity of nine electrodes along with error bars representing the various histograms. The data is accompanied by a relative standard deviation (RSD) of 5%, indicating a high level of reproducibility. The specificity of Ha006a/MCPE for atrazine was determined using interference experiments. We conducted a study to examine the impact of ATZ when combined with other pesticides, namely cypermethrin (Cyp), difenoconazole (Dif), chlorineuromethyl (Chl), tebuconazole (Teb), imidacloprid (Imi), metsulfuron-methyl (Met)). The DPV technique was used to determine the peak currents of all the species from the potential range of 0–0.6 V, based on Fig. 8b**.** The equivalent concentration of these interferants was 50 µM in 1 µM HCl buffer. The ATZ has a substantially greater peak current compared to other interfering species. Hence, the Ha006a/MCPE exhibits selectivity towards ATZ and thus can be effectively employed in practical implementation. The plot in Fig. 8c depicts the maximum current of ATZ and other species. The peak current, characterized by a standard variation of 5%, has little impact on the detection outcomes. Therefore, Ha006a/MCPE demonstrates satisfactory selectivity in detecting ATZ in the presence of typical interfering substances. The stability of the modified Ha006a/MCPE was assessed by cyclic voltammetry with 25 cycles in a solution of 0.1 M KCl/1 mM $[K_4Fe(CN)_6]$, with a potential range of − 0.2 to 0.6 V. Figure 8d shows a minimal decrease in peak current compared to the 1st and 25th cycle. Hence, the electrode is impervious to fouling.

Detection of atrazine in spiked and wastewater samples

The applicability of the developed sensor (Ha006a/MCPE) was validated through the detection of ATZ in various matrices, including wastewater from Sewage treatment plant (STP), milk and tap water samples. The wastewater sample was obtained from the campus wastewater treatment facility and centrifuged at 8000 rpm for 10 min to

Samples	Spiked concentration (μM)	Detected concentration (n-3)	Recovery (%)
STP water	6	5.74 ± 1.03	95.66
	12	11.66 ± 0.71	97.16
	18	17.59 ± 1.16	97.72
Tap water	6	5.89 ± 0.91	98.16
	12	11.84 ± 0.74	98.66
	18	17.68 ± 1.21	98.22
Milk samples	6	5.77 ± 0.88	96.16
	12	11.68 ± 1.27	97.33
	18	17.64 ± 1.08	98

Table 2. Recovery percentage of the sensor using real-time samples.

remove suspended particles. The milk sample was procured from a local shop and centrifuged at 10,000 rpm for 30 min before spiking. The supernatants of the wastewater sample, milk sample and tap water were then spiked with different concentrations of ATZ (6 μM, 12 μM and 18 μM). Peak current was noted and quantification was performed using the equation that depicts a straight line. Table 2 illustrates the real-world usefulness of the Ha006a/MCPE for detecting ATZ. The findings suggest that the rate of recovery was more significant in distilled water than in sewage water and milk. This is because several interfering substances are present in both the wastewater and milk samples. Therefore, the impact of interference was not significantly observed in the wastewater sample.

Conclusions

In summary, the carboxylesterase enzyme Ha006a was freshly purified and meticulously characterized using both biochemical and biophysical techniques to monitor its interaction with herbicide. The interaction between the Ha006a protein and ATZ was validated through initial docking results, confirming the association between the two. Consequently, the pure Ha006a protein was used to fabricate a durable electrochemical sensor for the remediation of the toxic pesticide atrazine. Experiments were conducted to optimize several parameters in electrochemical studies, such as the impact of scan rate, the influence of buffer solution, and its molarity. The Ha006a/MCPE exhibited remarkable performance in detecting ATZ, displaying excellent reproducibility, stability and selectivity. The sensor's real-time capability was assessed by detecting atrazine herbicide in tap water, sewage water and milk samples, resulting in high recovery. The developed sensor achieves a lower detection limit of 5.4 μM, which stands out favorably compared to cell-free sensors previously reported for detecting atrazine[16].

Moreover, our developed sensor exhibits a significantly higher limit of detection (LOD) in comparison to biosensors utilizing Ana-1 cells and aptamers for detecting atrazine[35,36]. Hence, Ha006a protein exhibited excellent performance as the enzyme-based biosensor and paved the way for its utilization in the identification of other herbicides. Furthermore, it can be utilized to develop a portable and adaptable device capable of identifying ATZ and performing real-time monitoring of various samples such as wastewater, milk and drinking water. Inline analyte detection in water requires developing sensing probes and packaging specifically designed for the intended use. It is imperative to develop a revamped calibration system to facilitate such detection and we are already making significant progress in this regard.

Data availability

The data that support the findings of this study are available from [Prof Praveen C Ramamurthy]. Still, restrictions apply to the availability of these data, which were used under license for the current study and are not publicly available. However, data are available from the authors upon reasonable request and with permission of [Prof Praveen C Ramamurthy].

Received: 1 March 2024; Accepted: 24 June 2024
Published online: 26 July 2024

References

1. Mili, C., Kalita, S. & Roy, S. Microbes as a potential bioremediation tool for atrazine-contaminated soil: A review. *J. Appl. Biol. Biotechnol.* **11**, 8–15 (2023).
2. Zhang, F. *et al.* Enhanced phytoremediation of atrazine-contaminated soil by vetiver (*Chrysopogon zizanioides* L.) and associated bacteria. *Environ. Sci. Pollut. Res.* **30**, 44415–44429 (2023).
3. Hwang, J.-I. & Wilson, P. C. Absorption, translocation, and metabolism of atrazine, carbamazepine, and sulfamethoxazole by the macrophyte Orange King Humbert canna lily (*Canna* × *generalis* LH Bailey (pro sp) [*glauca* × *indica*]). *Environ. Sci. Pollut. Res.* **30**, 46282–46294 (2023).
4. Prathap, M. & Udayan, A. Electrochemical detection of herbicide atrazine using porous MnO_2-NiO nanocatalyst. *Mater. Sci. Eng. B* **290**, 116302 (2023).
5. Supraja, P., Singh, V., Vanjari, S. R. K. & Govind Singh, S. Electrospun CNT embedded ZnO nanofiber based biosensor for electrochemical detection of Atrazine: A step closure to single molecule detection. *Microsyst. Nanoeng.* **6**, 1–10 (2020).
6. Simpkins, J. W. *et al.* Atrazine and breast cancer: A framework assessment of the toxicological and epidemiological evidence. *Toxicol. Sci.* **123**, 441–459 (2011).
7. Almberg, K. S. *et al.* Atrazine contamination of drinking water and adverse birth outcomes in community water systems with elevated atrazine in Ohio, 2006–2008. *Int. J. Environ. Res. Public Health* https://doi.org/10.3390/ijerph15091889 (2018).

8. Stutz, H., Pittertschatscher, K. & Hans, M. Capillary zone electrophoretic determination of hydroxymetabolites of atrazine in potable water using solid-phase extraction with amberchrom resins. *Mikrochim. Acta* **128**, 107–117 (1998).
9. Steinheimer, T. R. HPLC determination of atrazine and principal degradates in agricultural soils and associated surface and ground water. *J. Agric. Food Chem.* **41**, 588–595 (1993).
10. Ma, W. T., Fu, K. K., Cai, Z. & Jiang, G. B. Gas chromatography/mass spectrometry applied for the analysis of triazine herbicides in environmental waters. *Chemosphere* **52**, 1627–1632 (2003).
11. Bilal, S. *et al.* An insect acetylcholinesterase biosensor utilizing WO3/g-C3N4 nanocomposite modified pencil graphite electrode for phosmet detection in stored grains. *Food Chem.* **346**, 128894 (2021).
12. Bilal, S. *et al.* A novel construct of an electrochemical acetylcholinesterase biosensor for the investigation of malathion sensitivity to three different insect species using a $NiCr_2O_4$/g-C_3N_4 composite integrated pencil graphite electrode. *RSC Adv.* **12**, 16860–16874 (2022).
13. Alberti, G., Zanoni, C., Spina, S., Magnaghi, L. R. & Biesuz, R. MIP-based screen-printed potentiometric cell for atrazine sensing. *Chemosensors* **10**, 339 (2022).
14. Tortolini, C., Bollella, P., Antiochia, R., Favero, G. & Mazzei, F. Inhibition-based biosensor for atrazine detection. *Sens. Actuators B Chem.* **224**, 552–558 (2016).
15. Švorc, Ľ, Rievaj, M. & Bustin, D. Green electrochemical sensor for environmental monitoring of pesticides: Determination of atrazine in river waters using a boron-doped diamond electrode. *Sens. Actuators B Chem.* **181**, 294–300 (2013).
16. Silverman, A. D., Akova, U., Alam, K. K., Jewett, M. C. & Lucks, J. B. Design and optimization of a cell-free atrazine biosensor. *ACS Synth. Biol.* **9**, 671–677 (2020).
17. Liu, X. *et al.* A label-free electrochemical immunosensor based on gold nanoparticles for direct detection of atrazine. *Sens. Actuators B Chem.* **191**, 408–414 (2014).
18. Liu, R., Guan, G., Wang, S. & Zhang, Z. Core-shell nanostructured molecular imprinting fluorescent chemosensor for selective detection of atrazine herbicide. *Analyst* **136**, 184–190 (2010).
19. Kaur, H. *et al.* Heterologous expression, biochemical characterization and prospects for insecticide biosensing potential of carboxylesterase Ha006a from *Helicoverpa armigera*. *Pestic. Biochem. Physiol.* https://doi.org/10.1016/J.PESTBP.2024.105844 (2024).
20. Jumper, J. *et al.* Highly accurate protein structure prediction with AlphaFold. *Nature* **596**, 583–589 (2021).
21. Lu, S. *et al.* CDD/SPARCLE: The conserved domain database in 2020. *Nucleic Acids Res.* **48**, D265–D268 (2020).
22. Kim, S. *et al.* PubChem 2023 update. *Nucleic Acids Res.* **51**, D1373–D1380 (2023).
23. O'Boyle, N. M. *et al.* Open Babel: An open chemical toolbox. *J. Cheminform.* **3**, 33 (2011).
24. Trott, O. & Olson, A. J. AutoDock Vina: Improving the speed and accuracy of docking with a new scoring function, efficient optimization, and multithreading. *J. Comput. Chem.* https://doi.org/10.1002/jcc.21334 (2009).
25. Morris, G. M. & Lim-Wilby, M. Molecular docking. *Methods Mol. Biol.* **443**, 365–382 (2008).
26. Seeliger, D. & De Groot, B. L. Ligand docking and binding site analysis with PyMOL and Autodock/Vina. *J. Comput. Aided Mol. Des.* **24**, 417–422 (2010).
27. Huang, J. & Mackerell, A. D. CHARMM36 all-atom additive protein force field: Validation based on comparison to NMR data. *J. Comput. Chem.* **34**, 2135–2145 (2013).
28. Hanwell, M. D. *et al. SOFTWARE Open Access Avogadro: An Advanced Semantic Chemical Editor, Visualization, and Analysis Platform*. *Journal of Cheminformatics* vol. 4. http://www.jcheminf.com/content/4/1/17 (2012).
29. Vanommeslaeghe, K., Raman, E. P. & MacKerell, A. D. Automation of the CHARMM General Force Field (CGenFF) II: Assignment of bonded parameters and partial atomic charges. *J. Chem. Inf. Model.* **52**, 3155–3168 (2012).
30. Van Der Spoel, D. *et al.* GROMACS: Fast, flexible, and free. *J. Comput. Chem.* **26**, 1701–1718. https://doi.org/10.1002/jcc.20291 (2005).
31. Paketurytė, V., Zubrienė, A., Ladbury, J. E. & Matulis, D. Intrinsic thermodynamics of protein-ligand binding by isothermal titration calorimetry as aid to drug design. *Methods Mol. Biol.* **1964**, 61–74 (2019).
32. Núñez, S., Venhorst, J. & Kruse, C. G. Target–drug interactions: First principles and their application to drug discovery. *Drug Discov. Today* **17**, 10–22 (2012).
33. Bissantz, C., Kuhn, B. & Stahl, M. A medicinal chemist's guide to molecular interactions. *J. Med. Chem.* **53**, 5061–5084 (2010).
34. Freire, E. Isothermal titration calorimetry: controlling binding forces in lead optimization. *Drug Discov. Today Technol.* **1**, 295–299 (2004).
35. Wang, X. *et al.* A sensitive and simple macrophage-based electrochemical biosensor for evaluating lipopolysaccharide cytotoxicity of pathogenic bacteria. *Biosens. Bioelectron.* https://doi.org/10.1016/j.bios.2016.03.007 (2016).
36. Ma, L. *et al.* Harnessing the affinity of magnetic nanoparticles toward dye-labeled DNA and developing it as an universal aptasensor revealed by lipopolysaccharide detection. *Anal. Chim. Acta* https://doi.org/10.1016/j.aca.2018.06.060 (2018).
37. Supraja, P., Tripathy, S., Krishna Vanjari, S. R., Singh, V. & Singh, S. G. Electrospun tin (IV) oxide nanofiber based electrochemical sensor for ultra-sensitive and selective detection of atrazine in water at trace levels. *Biosens. Bioelectron.* **141**, 111441 (2019).
38. Liu, B., Yan, J., Wang, M. & Wu, X. Molecularly imprinted electrochemical sensor for the detection of bisphenol A. *Int. J. Electrochem. Sci* **14**, 3610–3617 (2019).

Acknowledgements

Dr. Simranjeet Singh extends appreciation to the DBT HRD Project and Management Unit, Regional Center for Biotechnology, NCR Biotech Science Cluster, Faridabad, Haryana, for the Research Associateship (DBT-RA) and the corresponding funding outlined in award letter No DBT-RA/2022/July/N/2044 dated January 12, 2023. The authors express gratitude to the Ministry of Education (MoE) for their valuable support through the grant MoE-STARS/STARS-2/2023-0714, dated September 26, 2022.

Author contributions

Conceptualization, Methodology, Software, Data curation, Writing—Original draft: Supervision: Simranjeet Singh, Writing, Reviewing and Editing: Pavithra N, Harry Kaur, Radhika Varshney, Nadeem A Khan, Rakesh Kumar, Ashwani Kumar Sharma, Joginder Singh Visualization, Investigation, Software, Validation and Supervision: Praveen C. Ramamurthy. Harry Kaur & Pavithra N contributed equally to this work.

Competing interests

The authors declare no competing interests.

Additional information

Supplementary Information The online version contains supplementary material available at https://doi.org/10.1038/s41598-024-65801-y.

Correspondence and requests for materials should be addressed to P.C.R.